

NMR study of small molecule adsorption in MOF-74-Mg

M. G. Lopez,¹ Pieremanuele Canepa,¹ and T. Thonhauser^{1, a)}

Department of Physics, Wake Forest University, Winston-Salem, NC 27109, USA.

(Dated: 22 March 2022)

We calculate the carbon nuclear magnetic resonance (NMR) shielding for CO₂ and the hydrogen shieldings for both H₂ and H₂O inside the metal organic framework MOF-74-Mg. Our *ab initio* calculations are at the density functional theory level using the van der Waals including density functional vdW-DF. The shieldings are obtained while placing the small molecules throughout the structure, including the calculated adsorption site for various loading scenarios. We then explore relationships between loading, rotational and positional characteristics, and the NMR shieldings for each adsorbate. Our NMR calculations show a change in the shielding depending on adsorbate, position, and loading in a range that is experimentally observable. We further provide a simple model for the energy and the NMR shieldings throughout the cavity of the MOF. By providing this mapping of shielding to position and loading for these adsorbates, we argue that NMR probes could be used to provide additional information about the position at which these small molecules bind within the MOF, as well as the loading of the adsorbed molecule.

I. INTRODUCTION

Metal Organic Frameworks (MOFs)^{1–3} have become very popular over the last decade, as is evident by their prevalence in recent studies and generous review in the literature.^{4–11} This interest is largely due to the wide range of applications that have been identified for MOFs, ranging from molecular gas storage (CH₄,^{12–14} N₂,^{15,16} CO₂,^{16–19} H₂^{20–24}) to gas separation,^{25–29} drug delivery,^{30,31} sensing,^{32,33} catalysis,^{34–40} and photocatalysis.^{41,42} The utility of MOFs comes from their interactions with small molecules such as H₂, CO₂, and H₂O. It is thus critical to understand the details of the binding process when a small molecule is adsorbed into the MOF. To this end, IR and Raman spectroscopy have been used extensively to study small molecule adsorption in MOFs,^{43–45} but it can be difficult to determine where the reactive sites reside under different loading scenarios. Also, for these probes the strong signals originating from the vibrational modes of the gas present in the experiment chamber and the MOF itself can often dominate the spectrum, making the analysis of the weak adsorbate signal challenging. In the following, we argue that NMR—which has already been used successfully to study MOFs in a number of cases^{46–51}—can be used to facilitate a more detailed understanding of the static behavior of MOF/adsorbate interactions and binding under various conditions. In particular, we show that NMR can provide information about the position at which these small molecules bind within the MOF, as well as the loading of the adsorbed molecule.

In this work, we consider the particular MOF structure MOF-74-Mg,⁵² which has been shown to have very high efficiency when capturing CO₂,²⁶ a key property for gas separation and storage applications. For the small molecule adsorbed in the MOF we consider H₂, CO₂,

and H₂O. The first is obviously interesting for hydrogen-storage applications, while the second one is of interest in carbon-capture applications. However, water by itself is not necessarily interesting for applications, were it not for the fact that it strongly impedes the performance in the first two cases. In other words, the presence of water, due to its strong binding characteristics, decreases the performance of MOFs in hydrogen-storage and CO₂ capture applications, such that its careful study is warranted.⁵³

The three molecules investigated in this study, i.e. H₂, CO₂, and H₂O, bind inside the MOF through physisorption. Thus, it is apparent that the proper inclusion of van der Waals interactions is crucial for the entire study. Therefore, we use density functional theory (DFT), utilizing the van der Waals including functional vdW-DF^{54–56} to map the shielding of an adsorbed molecule within MOF-74-Mg to various characteristics. This truly non-local exchange-correlation functional has already successfully been applied to study small molecule adsorption in a variety of MOFs.^{43–45,53,57–64}

II. COMPUTATIONAL DETAILS

The interaction of H₂, CO₂, and H₂O with MOF-74-Mg was studied using DFT with vdW-DF as implemented in QUANTUMESPRESSO.⁶⁵ It is well known that binding distances will usually be slightly overestimated using vdW-DF.⁵⁶ We used the primitive rhombohedral unit cell of MOF-74-Mg with space group R $\bar{3}$ and 54 atoms. The initial geometry of MOF-74-Mg was relaxed, fixing the lattice parameters according to the experimental values of $a = 15.117 \text{ \AA}$ and $\alpha = 117.742^\circ$.¹⁴ A complete volume relaxation for all loadings considered in this paper would have been extremely computationally expensive, so that we fixed the lattice constants to the experimentally measured ones. In our testing, for the expected worse case of 12 H₂O molecules adsorbed in MOF-74-Mg, we find that there is only a 1%

^{a)}E-mail: thonhauser@wfu.edu

change in the channel diameter when a full relaxation is performed. For each adsorption case we have relaxed the internal coordinates until the total force was below 1×10^{-4} Ry Bohr $^{-1}$. Ultrasoft pseudopotentials together with a plane-wave cutoff of 35 Ry were used to describe the wave functions, while the charge-density cutoff was set to 280 Ry. The convergence threshold for the self-consistency of the total energy was set to 5×10^{-11} Ry, ensuring an accurate sampling of the complex potential energy surface for MOF-74-Mg.

With the coordinates obtained from the geometry relaxation, the adsorption energies and NMR shielding parameters were calculated using norm-conserving GIPAW pseudopotentials,⁶⁶ which allow for the wavefunction reconstruction in the atomic core region. Structural aspects are not so sensitive to the cutoffs, ensuring the lower values reported above for the geometry optimizations are appropriate. But, the NMR shielding parameters are much more sensitive, so that higher values are needed. Accordingly, we used a plane-wave cutoff of 120 Ry and a charge-density cutoff of 420 Ry, resulting in a convergence of the absolute shielding to within 0.05 ppm. However, in this study we are mostly interested in the *change* in shielding of the adsorbed molecule compared to its gas phase, which is converged to within less than 0.001 ppm. For the NMR shielding calculations,⁶⁷ we used a combination of the linear-response⁶⁸ and new converse^{69–71} methods—the latter being built entirely on the theory of orbital magnetization.^{72–75} The adsorption energies reported in this study were calculated with identical parameters to these NMR calculations.

In addition, we cross-checked our calculated NMR shieldings for selected adsorption cases of H₂ with VASP⁷⁶ (a plane-wave code) and GAUSSIAN⁷⁷ localized basis-set code). We find that the gas-phase shieldings of those codes agree to within less than 0.1 ppm with our results, but more importantly, the shielding difference between gas-phase and adsorbed molecules agrees with our calculations to within 0.01 ppm.

III. RESULTS

A. Reactivity and binding energy

Although the subject of the binding characteristics itself is not the main focus of this study, we reproduce and extend results here that have been published elsewhere⁵³ but are nonetheless important for our NMR study. In particular, the adsorption energy of H₂, CO₂, and H₂O in MOF-74-Mg under different loading situations is of interest, as it defines the primary and secondary binding sites and binding geometries, for which we will report NMR results below. The structure of MOF-74, which can be seen in Figs. 1 and 2, consists of hexagonal channels, where metal atoms at the corners are connected by benzenedicarboxylate linkers. The primary binding sites

TABLE I. Adsorption energies ΔE of molecules in MOF-74-Mg in eV for different loadings. ΔE_{prim} and ΔE_{sec} are the average adsorption energies for the molecule at the primary and secondary binding sites, respectively. ΔE_{avg} is the average adsorption energy per molecule considering all adsorbed molecules together.

M	Loading	ΔE_{prim}	ΔE_{sec}	ΔE_{avg}
H ₂	1	-0.15	n/a	-0.15
	6	-0.16	n/a	-0.16
	7	-0.16	-0.12	-0.15
	12	-0.16	-0.12	-0.14
CO ₂	1	-0.50	n/a	-0.50
	6	-0.50	n/a	-0.50
	7	-0.50	-0.43	-0.49
	12	-0.50	-0.46	-0.48
H ₂ O	1	-0.79	n/a	-0.79
	6	-0.76	n/a	-0.76
	7	-0.74	-0.61	-0.72
	12	-0.74	-0.65	-0.70

are located near the six metal ions in each unit cell, while secondary binding sites are nearer to the linkers. For further details, see Ref. 53.

The adsorption energy, ΔE , of a guest molecule M in the MOF is defined as

$$\Delta E = E_{\text{MOF}+\text{M}} - [E_{\text{MOF}} + E_{\text{M}}], \quad (1)$$

where E_{MOF} and E_{M} are the energies of the MOF and the molecule in their fully relaxed form, and $E_{\text{MOF}+\text{M}}$ is the energy of the MOF with the adsorbed M. Results for the adsorption energies ΔE are given in Table I for several different loadings: (i) *low loading*, i.e. one guest molecule per cell occupying a primary binding site; (ii) *high loading*, six guest molecules per cell completely saturating all available primary sites; (iii) *high loading*, 7 guest molecules per cell completely saturating all primary sites and one secondary site; and (iv) *very high loading*, 12 molecules per unit cell, occupying all available primary and secondary binding sites. For a depiction of the binding geometries in those cases, see Fig. 1. We find good agreement with the experimental adsorption energies of -0.11 ± 0.003 eV for H₂⁷⁸ and -0.49 ± 0.010 eV for CO₂,⁷⁹ attesting to the importance of correctly including van der Waals interactions in these simulations. In a recent study⁵³ we also computed vibrational frequencies to obtain the thermal and zero-point energy (ZPE) corrections to these adsorption energies, allowing for a more accurate comparison to measured adsorption heats. But, for the cases considered here, we found that these corrections are on the order of 0.01 eV or less, so they are not again reported here.

The influence of “crowding” on the adsorbed molecules in high-loading situations is present, but not dominating. For H₂, the contribution of the lateral interactions in the high-loading scenarios is negligible, being less than 7% of

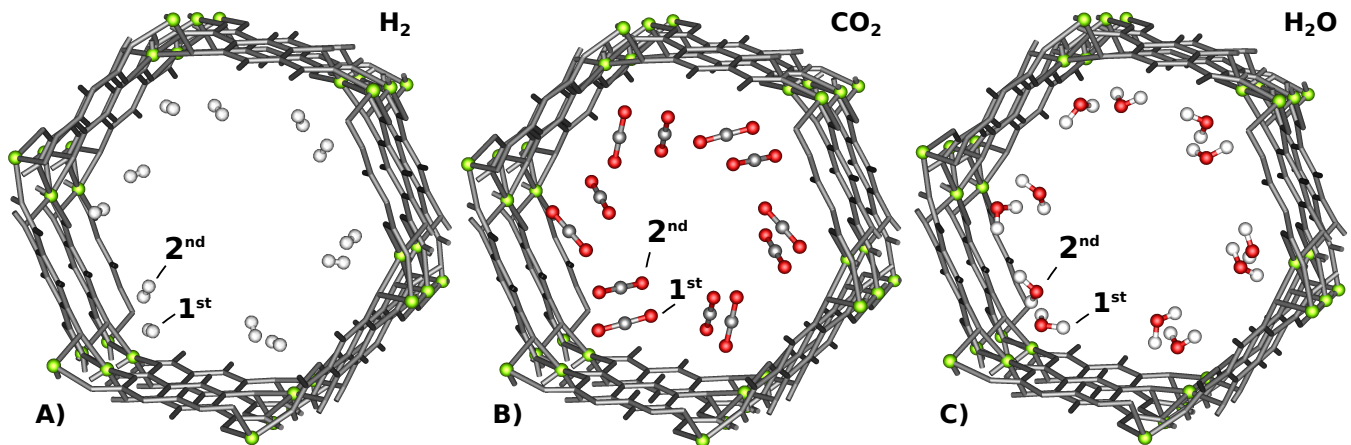


FIG. 1. The MOF-74-Mg structure is shown as sticks with metal Mg ions highlighted as green balls. The three panels show A) H₂, B) CO₂, and C) H₂O as ball-and-stick representations in the case of very high loading with all six primary and all six secondary binding sites occupied, labelled as 1st and 2nd, respectively. Notice the classic dimer configuration of the adsorbed water molecules.

the total binding energy in the case of 12 adsorbed H₂ molecules. For the CO₂ and H₂O molecules, the lateral interactions (attractive) contribute less than 10% of the total binding energy as given in Table I when only each of the six primary binding sites is occupied. However, when all available primary and secondary sites are occupied (12 molecules bound), this contribution increases to 18% and 25% for CO₂ and the hydrogen bonding H₂O cases, respectively.

B. NMR – Loading study

We now move to the main topic of this study—the analysis of the NMR chemical shielding of H₂, CO₂, and H₂O in MOF-74-Mg. Unless otherwise stated, the reported values in parts per million (ppm) are the *change* in isotropic NMR chemical shielding $\Delta\sigma$ when the gas-phase molecule M is adsorbed in the MOF, i. e.

$$\Delta\sigma = \sigma_{M \text{ in MOF}} - \sigma_{M \text{ in gas phase}} \quad (2)$$

After determining the primary and secondary binding sites for the three adsorbate molecules in the different loading cases (see Sec. III A), we calculated the NMR shielding of the adsorbed molecules at those positions within the MOF-74-Mg structure; corresponding values are reported in Table II. In primary and secondary site high-loading cases, the average of equivalent atoms is reported. When a single secondary site is occupied by water, it forms a classic water dimer by hydrogen bonding with the water at the nearest primary binding site. For this reason, only the five unpaired primary sites are averaged in Table II for H₂O with a loading of 7; the values of the “special” molecule, to which the seventh molecule in the secondary binding site attaches, are reported separately.

The chemical shielding dependence on adsorbate loading can be seen in Table II for all three molecules. It

is perhaps not surprising to see that while H₂ shows a typically weak vdW physisorption-like interaction with the MOF (also indicated by the smaller binding energies in Table I), water displays the more typical proton NMR deshielding behavior. When H₂O occupies any of the secondary binding sites, it assumes a dimer configuration with the molecule in the primary site with an average hydrogen-bond distance of 1.86 Å which is consistent with previous results.⁸⁰ This hydrogen bonding produces a large effect which can be seen by large shielding changes for H₂O in high-loading cases shown in Table II. These large shielding changes are in good agreement with previous NMR studies of liquid water in which hydrogen bonding also plays a significant role.^{70,81} While it is conceivable that as the loading increases, the water molecules could form a hydrogen-bond chain instead of occupying the remaining secondary binding sites in the cell, calculations and experiment⁸⁰ indicate that the hydrogen bond only accounts for about one third of the secondary site binding energy, making this configuration less favorable.

From these results, it can be seen that—while direct usage of NMR alone to determine relative loadings for H₂ might be difficult—the situation is more positive for CO₂ and H₂O. For CO₂, relative loadings of the primary binding site show up clearly as a significant difference. While the differences are not as obvious for the secondary site, the presence of two peaks—one around 1 ppm and another greater than 2 ppm from the gas phase shieldings is a good indication of CO₂ occupying both primary and secondary sites. For H₂O, the changes in shieldings at the primary binding site (in the absence of hydrogen bonding) are much smaller as loading increases, but the presence of low loadings can still be detected with a change in shielding around 0.8 ppm less than the gas phase value. Furthermore, the formation of hydrogen bonds when greater than six molecules are adsorbed is a clear indication of high-loading situations for H₂O.

TABLE II. Change in NMR shielding $\Delta\sigma$ in ppm (carbon for CO_2 , hydrogen for H_2 and H_2O) upon adsorption relative to the gas phase for the primary and secondary binding sites. Shieldings for the primary and secondary binding sites are given in separate columns. For H_2 and H_2O the values for both hydrogens are given in separate lines. In the cases of H_2 and H_2O , the first row is the hydrogen which is more strongly interacting with the oxygen plane of the metal binding site complex, while the second is further away. For higher loading situations, the shieldings have been averaged over all equivalent sites.

Loading	1		6		7		12	
	prim.	sec.	prim.	sec.	prim.	sec.	prim.	sec.
H_2	0.48	0.50	0.54	0.09	0.25	0.14		
	0.24	0.30	0.26	0.50	0.51	0.58		
CO_2	1.01	2.42	2.16	0.95	2.69	0.81		
H_2O	-0.83	-0.85	-1.06 ^a	-4.41	-0.53	-3.65		
	-0.74	-0.56	-0.78 ^a	-0.37	-5.42	-0.12		

^a -0.57 and -4.99 ppm for the molecule to which the seventh H_2O attaches.

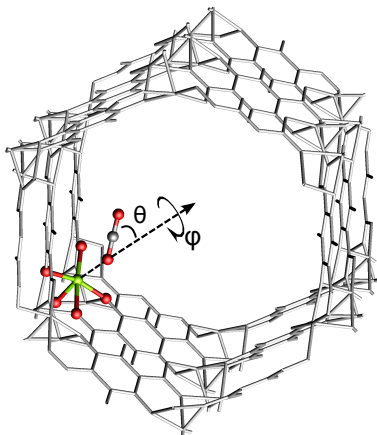


FIG. 2. Schematic drawing defining the rotation and its axis, depicted for the case of CO_2 . The molecule is placed at one of six identical primary binding sites, emphasized by the colored ball-and-stick representation with carbon, oxygen and magnesium represented as grey, red, and green balls, respectively. The axis of rotation is the polar axis defined as a line from the binding Mg through the closest atom of the small molecule. The molecule is then rigidly rotated (indicated by the curved arrow) about this axis, sampling the azimuthal angle $\varphi = 0 - 360^\circ$ and keeping θ fixed at its computed value in the lowest energy configuration—approximately 94° and 55° for H_2 and CO_2 , respectively.

C. NMR – Rotational study

Strictly speaking, Table II gives the NMR shielding change for molecules at the primary and secondary binding sites at zero temperature. However, for finite temperatures the molecules will start to “wiggle”—governed by the potential energy surface around the binding site—

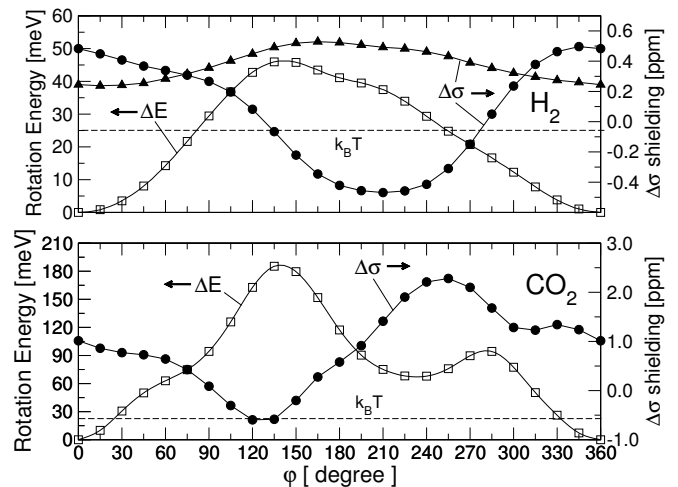


FIG. 3. The change in energy and NMR shielding calculated for H_2 and CO_2 as a function of rotation at the primary binding site in MOF-74-Mg. For H_2 , the shielding for both atoms is shown, with the fixed hydrogen shown as solid triangles and the rotated hydrogen with solid circles. For a definition of the angle and axis of rotation, see Fig. 2. The energy scale is shown on the left and the NMR shielding scale is on the right. The dashed lines indicate $k_B T$ at room temperature, i. e. 25.6 meV.

resulting in small changes in shielding. In order to investigate the order of magnitude of such changes, we studied the rotational (and in the next section, translational) behavior of H_2 and CO_2 at the primary binding site. The axis of rotation is defined by an imaginary line between the Mg atom and the closest hydrogen in H_2 or the closest oxygen in CO_2 at the binding site, as shown in Fig. 2 for CO_2 . The binding geometry is the lowest energy geometry and defines the zero-degree configuration for the azimuthal angle φ in Figs. 2 and 3. The relative angle θ was then “frozen” and the molecule was rotated from $\varphi = 0^\circ$ to $\varphi = 360^\circ$ in intervals of 15° . Note that this rotation is not meant to accurately sample energies and shieldings of physically likely situations—rather, it should give an estimate for the sensitivity of these properties in close proximity of the binding site.

In Fig. 3 we show both the energy and NMR shielding as the molecules are rotated 360° . Our results show that for H_2 at room temperature, there is a variation in the shielding by as much as 0.8 ppm, and at elevated temperatures as much as 1 ppm. For CO_2 at room temperature, there is a variation in the shielding up to 0.4 ppm, but at very high temperatures this variation can grow as large as 2.5 ppm. Note that there is a secondary minimum in the rotational energy for CO_2 around 230° , so that low temperature measurements could detect a secondary peak around 2 ppm further from the gas-phase shift. This secondary minimum has a depth of 30 meV and thus can maintain trapped molecules in this rotational configuration at room temperature.

D. NMR – Positional study

In the previous section we investigated the sensitivity of energy and shielding in the proximity of the binding site for simple rotations. In the following, we investigate the same for large deviation from the binding site—in fact, we calculate the energy and shielding change throughout the entire cavity of the MOF. In Figs. 4, 5, and 6 we show a map of the energies and NMR shieldings calculated for the small molecules at different positions within the cavity of MOF-74-Mg. The values shown are the change in shielding when the molecules are taken from gas phase into the MOF in a low-loading scenario. The planes over which the shielding was studied are defined by three points: the center of mass of the MOF-74-Mg unit cell, the binding site of the small molecule as calculated by the geometry relaxations described in Sec. II, and the Mg atom at which the molecule is adsorbed. Note that a plane defined in this way is not coplanar with the MOF structure, the normal vector to the plane being slightly tilted (by $10^\circ - 15^\circ$) away from the channel direction. This implies that replicating the NMR maps displayed in these figures using the D_{3d} symmetry of the MOF would yield a slightly discontinuous image. The values were calculated at 26 equidistant points within this plane and linear interpolation was used to make the complete map. At each of the sampled points, the center atom of the molecule was “pinned” to the location of interest, and the remaining atoms allowed to relax so that the molecule adopted its lowest energy orientation and internal geometry. The row of sampled points in the plane closest to the MOF were found to have energies for all molecules of more than 2.4 eV greater than the binding site, making it unphysical for the molecule to sample these regions even under high temperature and pressure situations.

By definition, at the binding sites the plotted values coincide with the values in Table II. Around the primary binding site in the energy map we have also indicated the 25.6 meV isoline ($k_B T$ at room temperature), which gives an estimate for the extent of spatial fluctuations of the molecules at room temperature. Note that we have also transferred this “fluctuation region” to the NMR maps, where they can now be used to estimate the fluctuations of the shielding change that can be expected at room temperature. However, it turns out that in all three cases these fluctuations are small.

It is also interesting to see that even in the middle of the MOF all guest molecules show a shielding significantly different from their gas phase. Although at that point the molecules are far away from the inside wall of the MOF, they are effectively surrounded by twelve benzene-like linkers (see the setup in Fig. 1), the π clouds of which influence the electronic structure of the adsorbed molecules. In the case of H_2 we investigated this behavior further with simple model calculations using GAUSSIAN with a 6-311++G(2d,2p) basis set: “Approximating” the MOF with 12 benzene rings and putting the H_2 in the

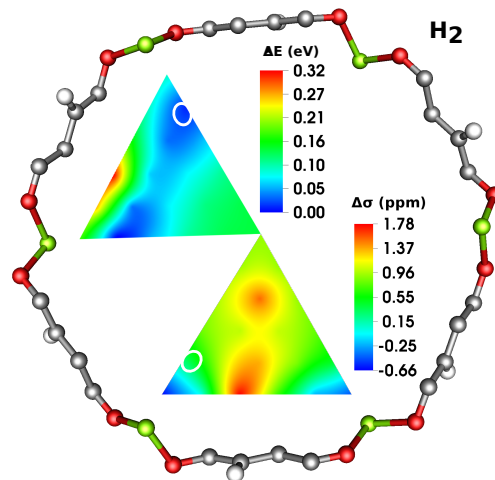


FIG. 4. Each triangle shows a map of the change in i) energy and ii) the NMR shielding as the H_2 molecule is moved throughout the cavity of MOF-74-Mg. The MOF is oriented so that the viewer is looking along the direction of the channel, and hydrogen, carbon, oxygen, and magnesium atoms are represented as white, grey, red, and green balls, respectively. The two maps were calculated at identical points, but they are shown here in symmetry-equivalent locations within the MOF structure for better comparison. The shielding is averaged over both hydrogen atoms. The energy is plotted relative to the binding energy. The white circle indicates $k_B T$ at room temperature, i. e. 25.6 meV, and is thus an estimate for the region around the primary binding site accessible through translational fluctuations at room temperature.

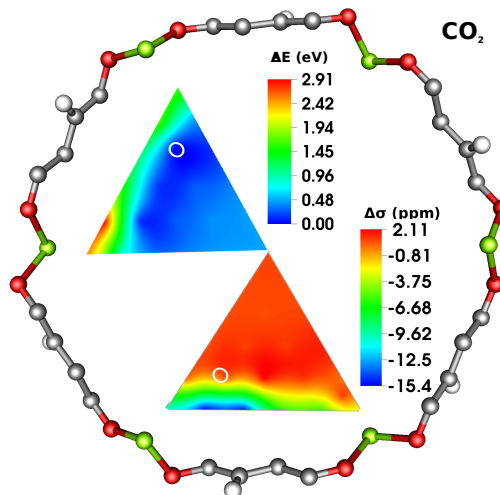


FIG. 5. Same as Fig. 4, but here for CO_2 .

center we find a difference in shielding to the gas phase of 0.91 ppm, whereas the full calculation with the periodic MOF structure using QUAANTUMESPRESSO gives 0.92 ppm.

For H_2 and H_2O , Figs. 4 and 6 suggest qualitatively similar behavior of the shielding for displacements near the binding site. However, as indicated in Table II and

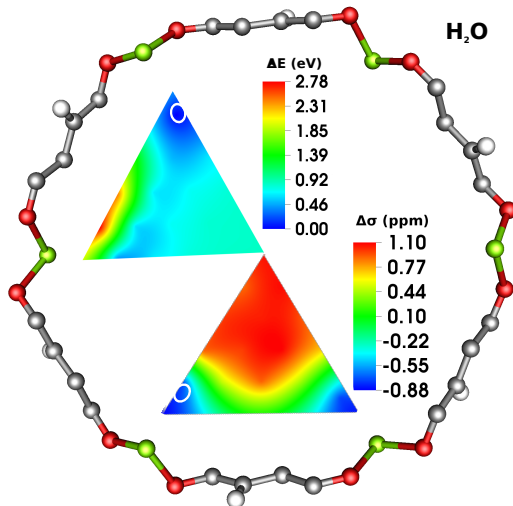


FIG. 6. Same as Fig. 4, but here for H₂O.

Figs. 4 and 6, while H₂O binds closer to the MOF (compare indicated positions of the binding sites in the maps) and deshields relative to the gas phase, H₂ binds slightly further away, although when forced closer to the metal ion site it also deshields.

Note that there is not a monotonic increase for either the energy or shielding when moving the small molecule from the center towards the MOF. The true function of shielding and energy throughout the cavity of the MOF is quite complicated, but we provide here a simple model to approximate both. To this end, we mimic the energy in the plane by a simple two-dimensional function (of r and ϕ in polar coordinates) inspired by a Lennard-Jones potential with angular dependence, i. e.

$$\Delta E = \left[\frac{a}{(r_0 - r)^x} - \frac{a}{(r_0 - r)^{x/2}} \right] \left[1 - b \sin^2(f\phi) \right] + E_0. \quad (3)$$

Here, r is the distance from the center of the MOF and ϕ is the polar angle. The zero angle is half-way between two Mg atoms. It turns out that a very similar model can also accommodate the spatial change in NMR shielding fairly well with only a minor modification, although there is no intuitive reason to believe the shielding should behave radially in a Lennard-Jones manner. For the shielding model, we reuse the energy model with the addition of a radial dependence in the angular piece of the function,

$$\Delta\sigma = \left[\frac{a}{(r_0 - r)^x} - \frac{a}{(r_0 - r)^{x/2}} \right] \left[1 - rb \sin^2(f\phi) \right] + \sigma_0. \quad (4)$$

These models were tested against the positional data used for the interpolation shown in Figs. 4–6, but only the originally sampled points were used in the parameter fitting. The parameters found for all three adsorbed molecules using both models are shown in Table III, along with the resulting mean absolute error (MAE) in either units of eV or ppm, as appropriate.

TABLE III. Parameters for the models described in Eqs. (3) and (4), along with the resulting mean absolute error (MAE), in either units of eV or ppm as appropriate, when compared to the original data.

		a	f	x	r_0	b	E_0, σ_0	MAE
ΔE	H ₂	0.64	2.79	3.43	6.83	0.67	0.15	0.02
	CO ₂	1.85	4.84	2.70	6.50	1.07	0.48	0.19
	H ₂ O	5.59	3.12	10.1	6.74	2.18	0.86	0.15
$\Delta\sigma$	H ₂	-1.76	-2.02	4.24	7.27	0.93	0.98	0.19
	CO ₂	10.1	0.61	17.8	6.75	-1.84	1.01	0.21
	H ₂ O	-0.19	-1.91	5.86	7.03	16.3	1.00	0.17

In both models, there appear to be six free parameters, but some further simplifications can be made. First, there is an overall shift parameter denoted by E_0 and σ_0 in Eq. (3) and Eq. (4), respectively. These values can be used in the fit minimization, but essentially turn out to be the value of the energy change ΔE or change in shielding $\Delta\sigma$ at the $r = 0$ point in the middle of the MOF. Hence, these values can be fixed accordingly in order to reduce the number of tuneable parameters in the model. Second, the r_0 parameter in all cases is within 1 Å of the distance from the middle of the MOF to the metal ion at the binding site and so could also be fixed, leaving only four overall adjustable parameters. We report in Table III these two parameters in addition to the remaining four so that the reader can get a sense of the magnitude and variance of these potentially “fixable” pieces of the model and more easily understand their roles in Eqs. (3) and (4).

We also find that the $\Delta\sigma$ model parameters for CO₂ reinforce what is shown in Fig. 5, i.e. that the shielding for CO₂ adsorbed in MOF-74-Mg behaves qualitatively differently from H₂ and H₂O. There is also a difference in the local adsorption geometry. Whereas both the H₂ and H₂O molecules adsorb “flat-on,” that is, almost parallel to the metal-oxygen plane which makes up the primary binding site, CO₂ adsorbs tilted upwards as explained in Sec. III C, pointing towards the Mg ion and interacting to a greater degree with the metal ion itself than with the oxygen plane. As pointed out in Ref. 79, the CO₂ does interact with the oxygens at the binding site so that its rotation is affected, but it is not “pulled over” to the extent that H₂ and H₂O are. Both the qualitative NMR behavior and adsorption geometry reflect a substantially different MOF-adsorbate interaction for the CO₂ case from the H₂ and H₂O cases.

IV. CONCLUSIONS

In summary, we have performed *ab initio* DFT simulations of the energy and NMR chemical shielding of H₂, CO₂, and H₂O in the MOF-74-Mg structure. Our calculations show that there is a relationship between loading

in MOF-74-Mg and the change in NMR shielding. While the loading dependence of the shielding is small, it still is within the measurable experimental range. We thus argue that combining the NMR signal strength with the peak positions can yield an accurate tool for determining the loading of MOFs. We have further shown how the energy and shielding behave as the molecules rotate or leave the binding site by providing detailed energies and NMR shieldings throughout the cavity of the MOF. From our calculated data, we were able to approximate the energies and shieldings with two simple functions. Although our study only investigated one particular MOF, we believe that the same approach is suitable for other MOFs and similar studies on e.g. MOF-5 and $\text{Zn}(\text{bdc})(\text{ted})_{0.5}$ are already in progress.

ACKNOWLEDGEMENTS

This work was supported in full by the Department of Energy Grant, Office of Basic Energy Sciences, Materials Sciences and Engineering Division, Grant No. DE-FG02-08ER46491.

- ¹B. Chen, M. Eddaoudi, S. T. Hyde, M. O’Keeffe, and O. M. Yaghi, *Science* **291**, 1021 (2001).
- ²M. Eddaoudi, H. Li, and O. M. Yaghi, *J. Am. Chem. Soc.* **122**, 1391 (2000).
- ³N. L. Rosi, J. Eckert, M. Eddaoudi, D. T. Vodak, J. Kim, M. O’Keeffe, and O. M. Yaghi, *Science* **300**, 1127 (2003).
- ⁴S. L. James, *Chem. Soc. Rev.* **32**, 276 (2003).
- ⁵G. Ferey, *Chem. Soc. Rev.* **37**, 191 (2008).
- ⁶M. O’Keeffe, *Chem. Soc. Rev.* **38**, 1215 (2009).
- ⁷J. J. Perry IV, J. A. Perman, and M. J. Zaworotko, *Chem. Soc. Rev.* **38**, 1400 (2009).
- ⁸S. S. Han, J. L. Mendoza-Cortes, and W. A. Goddard III, *Chem. Soc. Rev.* **38**, 1460 (2009).
- ⁹R. E. Morris and X. H. Bu, *Nat. Chem.* **2**, 353 (2010).
- ¹⁰H. Furukawa, N. Ko, Y. B. Go, N. Aratani, S. B. Choi, E. Choi, A. O. Yazaydin, R. Q. Snurr, M. O’Keeffe, J. Kim, and O. M. Yaghi, *Science* **329**, 424 (2010).
- ¹¹S. Bordiga, F. Bonino, K. P. Lillerud, and C. Lamberti, *Chem. Soc. Rev.* **39**, 488 (2010).
- ¹²M. Eddaoudi, J. Kim, N. Rosi, D. Vodak, J. Wachter, M. O’Keeffe, and O. M. Yaghi, *Science* **295**, 469 (2002).
- ¹³S. Q. Ma, D. F. Sun, J. M. Simmons, C. D. Collier, D. Q. Yuan, and H. C. Zhou, *J. Am. Chem. Soc.* **130**, 1012 (2008).
- ¹⁴H. Wu, W. Zhou, and T. Yildirim, *J. Am. Chem. Soc.* **131**, 4995 (2009).
- ¹⁵A. P. Nelson, O. K. Farha, K. L. Mulfort, and J. T. Hupp, *J. Am. Chem. Soc.* **131**, 458 (2009).
- ¹⁶K. Sumida, S. Horike, S. S. Kaye, Z. R. Herm, W. L. Queen, C. M. Brown, F. Grandjean, G. J. Long, A. Dailly, and J. R. Long, *Chem. Sci.* **1**, 184 (2010).
- ¹⁷P. D. C. Dietzel, R. E. Johnsen, H. Fjellvag, S. Bordiga, E. Groppo, S. Chavan, and R. Blom, *Chem. Commun.* **41**, 5125 (2008).
- ¹⁸D. M. D’Alessandro, B. Smit, and J. R. Long, *Angew. Chem. Int. Ed.* **49**, 6058 (2010).
- ¹⁹A. R. Millward and O. M. Yaghi, *J. Am. Chem. Soc.* **127**, 17998 (2005).
- ²⁰M. Dincă, A. Dailly, Y. Liu, C. M. Brown, D. A. Neumann, and J. R. Long, *J. Am. Chem. Soc.* **128**, 16876 (2006).
- ²¹P. M. Forster, J. Eckert, B. D. Heiken, J. B. Parise, J. W. Yoon, S. H. Jhung, J. S. Chang, and A. K. Cheetham, *J. Am. Chem. Soc.* **128**, 16846 (2006).
- ²²J. G. Vitillo, L. Regli, S. Chavan, G. Ricchiardi, G. Spoto, P. D. C. Dietzel, S. Bordiga, and A. Zecchina, *J. Am. Chem. Soc.* **130**, 8386 (2008).
- ²³L. J. Murray, M. Dincă, and J. R. Long, *Chem. Soc. Rev.* **38**, 1294 (2009).
- ²⁴Y. H. Hu and L. Zhang, *Adv. Mater.* **22**, E117 (2010).
- ²⁵J.-R. Li, R. J. Luppler, and H. C. Zhou, *Chem. Soc. Rev.* **38**, 1477 (2009).
- ²⁶D. Britt, H. Furukawa, B. Wang, T. G. Glover, and O. M. Yaghi, *Proc. Natl. Acad. Sci. U. S. A.* **106**, 20637 (2009).
- ²⁷H. Sato, R. Matsuda, K. Sugimoto, M. Takata, and S. Kitagawa, *Nat. Mater.* **9**, 661 (2010).
- ²⁸S. Shimomura, M. Higuchi, R. Matsuda, K. Yoneda, Y. Hijikata, Y. Kubota, Y. Mita, J. Kim, M. Takata, and S. Kitagawa, *Nat. Chem.* **2**, 633 (2010).
- ²⁹G. Ferey, C. Serre, T. Devic, G. Maurin, H. Jobic, P. L. Llewellyn, G. De Weireld, A. Vimont, M. Daturi, and J. S. Chang, *Chem. Soc. Rev.* **40**, 550 (2011).
- ³⁰B. Xiao, P. S. Wheatley, X. B. Zhao, A. J. Fletcher, S. Fox, A. G. Rossi, I. L. Megson, S. Bordiga, L. Regli, K. M. Thomas, and R. E. Morris, *J. Am. Chem. Soc.* **129**, 1203 (2007).
- ³¹P. Horcajada, T. Chalati, C. Serre, B. Gillet, C. Sebrie, T. Baati, J. F. Eubank, D. Heurtaux, P. Clayette, C. Kreuz, J. S. Chang, Y. K. Hwang, V. Marsaud, P. N. Bories, L. Cynober, S. Gil, G. Ferey, P. Couvreur, and R. Gref, *Nat. Mater.* **9**, 172 (2010).
- ³²Z. G. Xie, L. Q. Ma, K. E. deKrafft, A. Jin, and W. B. Lin, *J. Am. Chem. Soc.* **132**, 922 (2010).
- ³³S. L. Qiu and G. S. Zhu, *Coord. Chem. Rev.* **253**, 2891 (2009).
- ³⁴P. M. Forster and A. K. Cheetham, *Top. Catal.* **24**, 79 (2003).
- ³⁵B. Kesanli and W. B. Lin, *Coord. Chem. Rev.* **246**, 305 (2003).
- ³⁶J. Lee, O. K. Farha, J. Roberts, K. A. Scheidt, S. T. Nguyen, and J. T. Hupp, *Chem. Soc. Rev.* **38**, 1450 (2009).
- ³⁷L. Ma, C. Abney, and W. Lin, *Chem. Soc. Rev.* **38**, 1248 (2009).
- ³⁸A. Corma, H. Garcia, and F. X. Llabres i Xamena, *Chem. Rev.* **110**, 4606 (2010).
- ³⁹Y. Liu, W. M. Xuan, and Y. Cui, *Adv. Mater.* **22**, 4112 (2010).
- ⁴⁰H. L. Liu, Y. L. Liu, Y. W. Li, Z. Y. Tang, and H. F. Jiang, *J. Phys. Chem. C* **114**, 13362 (2010).
- ⁴¹K. E. Splan, A. M. Massari, and J. T. Hupp, *J. Phys. Chem.* **108**, 4111 (2004).
- ⁴²C. G. Silva, I. Luz, F. X. Llabres i Xamena, A. Corma, and H. Garcia, *Chem. Eur. J.* **16**, 11133 (2010).
- ⁴³K. Tan, N. Nijem, P. Canepa, Q. Gong, J. Li, T. Thonhauser, and Y. J. Chabal, *Chem. Mater.* **24**, 3153 (2012).
- ⁴⁴N. Nijem, H. Wu, P. Canepa, A. Marti, K. J. Balkus Jr., T. Thonhauser, J. Li, and Y. J. Chabal, *J. Am. Chem. Soc.* **134**, 15201 (2012).
- ⁴⁵N. Nijem, P. Canepa, L. Kong, H. Wu, J. Li, T. Thonhauser, and Y. J. Chabal, *J. Phys.: Condens. Matter* **24**, 424203 (2012).
- ⁴⁶F. Stallmach and J. Karger, *Chem. Mat. Sci.* **5**, 117 (1999).
- ⁴⁷O. Geier, R. Q. Snurr, F. Stallmach, and J. Karger, *J. Chem. Phys.* **120**, 367 (2004).
- ⁴⁸J. Gonzalez, R. N. Devi, D. P. Tunstall, P. A. Cox, and P. A. Wright, *Microporous and Mesoporous Materials* **84**, 97 (2005).
- ⁴⁹F. Stallmach, S. Groger, V. Kunzel, J. Karger, O. M. Yaghi, M. Hesse, and U. Muller, *Angewandte Chemie* **45**, 2123 (2006).
- ⁵⁰J. J. Gassensmith, H. Furukawa, R. A. Smaldone, R. S. Forgan, Y. Y. Botros, O. M. Yaghi, and J. F. Stoddart, *J. Am. Chem. Soc.* **133**, 15312 (2011).
- ⁵¹X. Kong, E. Scott, W. Ding, J. A. Mason, J. R. Long, and J. A. Reimer, *J. Am. Chem. Soc.* **134**, 14341 (2012).
- ⁵²P. D. C. Dietzel, R. Blom, and H. Fjellvag, *Eur. J. Inorg. Chem.* **23**, 3624 (2008).
- ⁵³P. Canepa, N. Nijem, Y. J. Chabal, and T. Thonhauser, *Phys. Rev. Lett.* **110**, 026102 (2013).
- ⁵⁴M. Dion, H. Rydberg, E. Schröder, D. C. Langreth, and B. I. Lundqvist, *Phys. Rev. Lett.* **92**, 246401 (2004).
- ⁵⁵T. Thonhauser, V. R. Cooper, S. Li, A. Puzder, P. Hyldgaard, and D. C. Langreth, *Phys. Rev. B* **76**, 125112 (2007).

- ⁵⁶D. C. Langreth, B. I. Lundqvist, S. D. Chakarova-Käck, V. R. Cooper, M. Dion, P. Hyldgaard, A. Kelkkanen, J. Kleis, L. Kong, S. Li, P. G. Moses, E. Murray, A. Puzder, H. Rydberg, E. Schröder, and T. Thonhauser, *J. Phys.: Condens. Mat.* **21**, 084203 (2009).
- ⁵⁷T. Sagara, J. Klassen, and E. Ganz, *J. Chem. Phys.* **123**, 214707 (2005).
- ⁵⁸A. M. Walker, B. Civalleri, B. Slater, C. Mellot-Draznieks, F. Cora, C. M. Zicovich-Wilson, G. Román-Pérez, J. M. Soler, and J. D. Gale, *Angew. Chem. Int. Ed.* **49**, 7501 (2010).
- ⁵⁹N. Nour, P. Thissen, Y. Yao, R. C. Longo, K. Roodenko, H. Wu, Y. Zhao, K. Cho, J. Li, D. C. Langreth, and Y. J. Chabal, *J. Am. Chem. Soc.* **133**, 12849 (2011).
- ⁶⁰L. Kong, Y. J. Chabal, and D. C. Langreth, *Phys. Rev. B* **83**, 121402(R) (2011).
- ⁶¹N. Nijem, J.-F. Veyan, L. Kong, H. Wu, Y. Zhao, J. Li, D. C. Langreth, and Y. J. Chabal, *J. Am. Chem. Soc.* **132**, 14846 (2010).
- ⁶²Y. Yao, N. Nijem, J. Li, Y. J. Chabal, D. C. Langreth, and T. Thonhauser, *Phys. Rev. B* **85**, 064302 (2012).
- ⁶³A. Centrone, D. Y. Siberio-Prez, A. R. Millward, O. M. Yaghi, A. J. Matzger, and G. Zerbi, *Chem. Phys. Lett.* **411**, 516 (2005).
- ⁶⁴A. Kuc, T. Heine, G. Seifert, and H. A. Duarte, *Chem. Eur. J.* **14**, 6597 (2008).
- ⁶⁵P. Giannozzi, S. Baroni, N. Bonini, M. Calandra, R. Car, C. Cavazzoni, D. Ceresoli, G. L. Chiarotti, M. Cococcioni, I. Dabo, A. Dal Corso, S. Fabris, G. Fratesi, S. de Gironcoli, R. Gebauer, U. Gerstmann, C. Gougoussis, A. Kokalj, M. Lazzeri, L. Martin-Samos, N. Marzari, F. Mauri, R. Mazzarello, S. Paolini, A. Pasquarello, L. Paulatto, C. Sbraccia, S. Scandolo, G. Sclauzero, A. P. Seitsonen, A. Smogunov P. Umari, and R. M. Wentzcovitch, *J. Phys.: Cond. Mat.* **39**, 395502 (2009).
- ⁶⁶C. J. Pickard and F. Mauri, *Phys. Rev. B* **63**, 245101 (2001).
- ⁶⁷Although the NMR parameters are being calculated for individual molecules, our calculations have shown that the so-called $G = 0$ contribution to the magnetic susceptibility related to the macroscopic shape of the sample does have a significant effect on the NMR results and needs to be included.
- ⁶⁸F. Mauri, B. G. Pfommer, and S. G. Louie, *Phys. Rev. Lett.* **77**, 5300 (1996).
- ⁶⁹T. Thonhauser, D. Ceresoli, and N. Marzari, *Int. J. Quantum Chem.* **109**, 3336 (2009).
- ⁷⁰T. Thonhauser, D. Ceresoli, A. A. Mostofi, N. Marzari, R. Resta, and D. Vanderbilt, *J. Chem. Phys.* **131**, 101101 (2009).
- ⁷¹D. Ceresoli, N. Marzari, M. G. Lopez, and T. Thonhauser, *Phys. Rev. B* **81**, 184424 (2010).
- ⁷²T. Thonhauser, *Int. J. Mod. Phys. B* **25**, 1429 (2011).
- ⁷³T. Thonhauser, D. Ceresoli, D. Vanderbilt, and R. Resta, *Phys. Rev. Lett.* **95**, 137205 (2005).
- ⁷⁴D. Ceresoli, T. Thonhauser, D. Vanderbilt, and R. Resta, *Phys. Rev. B* **74**, 024408 (2006).
- ⁷⁵R. Resta, D. Ceresoli, T. Thonhauser, and D. Vanderbilt, *ChemPhysChem* **6**, 1815 (2005).
- ⁷⁶G. Kresse and J. Furthmüller, *Phys. Rev. B* **54**, 11169 (1996); G. Kresse and D. Joubert, *Phys. Rev. B* **59**, 1758 (1999).
- ⁷⁷M. J. Frisch, G. W. Trucks, H. B. Schlegel, G. E. Scuseria, M. A. Robb, J. R. Cheeseman, G. Scalmani, V. Barone, B. Mennucci, G. A. Petersson, H. Nakatsuji, M. Caricato, X. Li, H. P. Hratchian, A. F. Izmaylov, J. Bloino, G. Zheng, J. L. Sonnenberg, M. Hada, M. Ehara, K. Toyota, R. Fukuda, J. Hasegawa, M. Ishida, T. Nakajima, Y. Honda, O. Kitao, H. Nakai, T. Vreven, J. A. Montgomery Jr., J. E. Peralta, F. Ogliaro, M. Bearpark, J. J. Heyd, E. Brothers, K. N. Kudin, V. N. Staroverov, R. Kobayashi, J. Normand, K. Raghavachari, A. Rendell, J. C. Burant, S. S. Iyengar, J. Tomasi, M. Cossi, N. Rega, J. M. Millam, M. Klene, J. E. Knox, J. B. Cross, V. Bakken, C. Adamo, J. Jaramillo, R. Gomperts, R. E. Stratmann, O. Yazyev, A. J. Austin, R. Cammi, C. Pomelli, J. W. Ochterski, R. L. Martin, K. Morokuma, V. G. Zakrzewski, G. A. Voth, P. Salvador, J. J. Dannenberg, S. Dapprich, A. D. Daniels, Ö. Farkas, J. B. Foresman, J. V. Ortiz, J. Cioslowski, and D. J. Fox, *Gaussian 09 Revision A.1*, Gaussian Inc. Wallingford CT 2009.
- ⁷⁸W. Zhou, H. Wu, and T. J. Yildirim, *J. Am. Chem. Soc.* **130**, 15268 (2008).
- ⁷⁹L. Valenzano, B. Civalleri, S. Chavan, G. T. Palomino, C. O. Areán, and S. Bordiga, *J. Phys. Chem. C* **114**, 11185 (2010).
- ⁸⁰B. Kolb and T. Thonhauser, *Phys. Rev. B* **84**, 045116 (2011).
- ⁸¹Note that there is a difference of sign convention between this work and the work in Ref. 70.